Rotational dynamics of solvated carbon dioxide studied by infrared, Raman, and time-resolved infrared spectroscopies and a molecular dynamics simulation

Kaori Watanabe, Hajime Okajima, Takuya Kato, and Hiro-o Hamaguchi

Citation: The Journal of Chemical Physics **136**, 014508 (2012); doi: 10.1063/1.3671998
View online: http://dx.doi.org/10.1063/1.3671998
View Table of Contents: http://scitation.aip.org/content/aip/journal/jcp/136/1?ver=pdfcov
Published by the AIP Publishing

Rotational dynamics of solvated carbon dioxide studied by infrared, Raman, and time-resolved infrared spectroscopies and a molecular dynamics simulation

Kaori Watanabe,[1] Hajime Okajima,[2] Takuya Kato,[1] and Hiro-o Hamaguchi[1,3,a)]
[1]*Department of Chemistry, School of Science, The University of Tokyo, Hongo 7-3-1, Bunkyo, Tokyo 113-0033, Japan*
[2]*Research Centre for Spectrochemistry, School of Science, The University of Tokyo, Hongo 7-3-1, Bunkyo, Tokyo 113-0033, Japan*
[3]*Institute of Molecular Science and Department of Applied Chemistry, National Chiao Tung University, Ta Hsueh Road 1001, Hsinchu 300, Taiwan*

(Received 12 October 2011; accepted 30 November 2011; published online 4 January 2012)

Rotational dynamics of solvated carbon dioxide (CO_2) has been studied. The infrared absorption band of the antisymmetric stretch mode in acetonitrile is found to show a non-Lorentzian band shape, suggesting a non-exponential decay of the vibrational and/or rotational correlation functions. A combined method of a molecular dynamics (MD) simulation and a quantum chemical calculation well reproduces the observed band shape. The analysis suggests that the band broadening is almost purely rotational, while the contribution from the vibrational dephasing is negligibly small. The non-exponential rotational correlation decay can be explained by a simple rotor model simulation, which can treat large angle rotations of a relatively small molecule. A polarized Raman study of the symmetric stretch mode in acetonitrile gives a rotational bandwidth consistent with that obtained from the infrared analysis. A sub-picosecond time-resolved infrared absorption anisotropy measurement of the antisymmetric stretch mode in ethanol also gives a decay rate that is consistent with the observed rotational bandwidths. © *2012 American Institute of Physics*. [doi:10.1063/1.3671998]

I. INTRODUCTION

Information on solvent-solute interactions is essential for in-depth understanding of chemical processes occurring in solution. Due to these interactions, the environment around the solute molecule varies in time with the motion of the solvent molecules and the fluctuation induced by the solvent motion either accelerates or decelerates the chemical processes. Vibrational band shape analysis provides a powerful tool for studying such dynamic interactions between the solvent and solute molecules. The fluctuation causes the dephasing of a vibration, which can be observed as a band broadening in the frequency domain.

Infrared and Raman band shapes have long been studied in order to acquire information on intermolecular solvent-solute interactions.[1–4] They are complementary with each other. While Raman spectroscopy can distinguish the contributions from vibrational and rotational dephasings via polarization measurements, infrared spectroscopy cannot. Thus, in past infrared band shape analyses, rotational dephasing has been most often treated as a slow diffusion process that gives a small band broadening.[5,6] Other methods such as time-resolved infrared absorption anisotropy,[7,8] dielectric relaxation,[9,10] spin relaxation,[11,12] and anisotropic fluorescence measurements[13,14] and MD simulations[15] are necessary in order to quantitatively estimate the rotational contribution to the observed infrared band shape.

This work aims at a comprehensive understanding of vibrational band shapes of small molecules in solution with a view to quantitative probing of intermolecular solvent-solute interactions. Infrared absorption, polarized Raman, and sub-picosecond time-resolved infrared absorption anisotropy measurements have been carried out with a combined theoretical analysis of a molecular dynamics simulation and a quantum chemical calculation. CO_2 has been chosen as a probe molecule for the following two reasons. First, it is a simple linear triatomic molecule with the three vibrational bands well separated in frequency. Second, it has no permanent dipole moment and is therefore soluble in various solvents, regardless of their polarity. The observed infrared band shape is discussed first, followed by an MD simulation/quantum chemical calculation analysis. Then, the result of polarized Raman measurements is discussed to confirm the theoretical analysis of the infrared band shape. Finally, sub-picosecond time-resolved infrared absorption anisotropy data are presented to further confirm the conclusion in the time domain.

II. THEORETICAL BASIS

A. Infrared band shape

An infrared band shape has contributions from both vibrational and rotational broadenings. The vibrational broadening is determined by vibrational dephasing due to the frequency modulation of the molecular vibration. Time-dependent vibrational frequency is separated into the mean

a)Author to whom correspondence should be addressed. Electronic mail: hhama@chem.s.u-tokyo.ac.jp.

value ω_0 and the fluctuation $\Delta\omega(t)$:

$$\omega(t) = \omega_0 + \Delta\omega(t). \tag{1}$$

Assuming that $\Delta\omega(t)$ follows a Markovian process, the vibrational correlation function can be expressed in the form:[16,17]

$$\phi_{\rm vib}(t) = \exp(i\omega_0 t)\left\langle \exp\left(i\int_0^\infty d\tau\,\Delta\omega(\tau)\right)\right\rangle. \tag{2}$$

The rotational broadening is determined by the reorientational motion of the molecule. It is represented by an autocorrelation of the unit vector $\boldsymbol{n}(t)$ fixed to the molecule:[18,19]

$$\phi_{\rm rot,IR}(t) = \langle \mathbf{n}(t)\cdot\mathbf{n}(0)\rangle\,. \tag{3}$$

Using the Wiener-Khinchin theory, the infrared band shape $I_{\rm IR}(\omega)$ is obtained by Fourier transforming the total correlation function; the product of the vibrational and rotational correlation functions,[16,17,20]

$$I_{IR}(\omega) = \int_{-\infty}^{\infty} dt\,\exp(-i\omega t)\cdot\phi_{vib}(t)\cdot\phi_{rot,IR}(t). \tag{4}$$

B. Computational method

A combined method of an MD simulation and a quantum chemical calculation[21] is employed to calculate the vibrational and rotational correlation functions. For the vibrational correlation function, frequency fluctuation $\Delta\omega$ [Eq. (1)] is parameterized in terms of the external electric field and the Van der Waals field as described in the following. Time-dependent field parameters are calculated from an MD simulation trajectory and then substituted into Eq. (2) to obtain the time-dependent vibrational frequency. Using this method, *ab initio* computations of the instantaneous frequency can be done at low computational cost, without repeating similar calculations. For the rotational correlation function, autocorrelation of the molecular axis [Eq. (3)] can be calculated directly from the MD simulation trajectory.

In order to parameterize the frequency fluctuation, $\Delta\omega$ is modeled to be a sum of fluctuations due to the long range Coulomb interaction ($\Delta\omega_{\rm CL}$) and the short-range Lennard-Jones (LJ) interaction ($\Delta\omega_{\rm LJ}$):

$$\omega(t) = \omega_0 + \Delta\omega = \omega_0 + \Delta\omega_{\rm CL} + \Delta\omega_{\rm LJ}. \tag{5}$$

$\Delta\omega_{\rm CL}$ is expanded in terms of the external electric field E_α on the carbon atom up to the second order:

$$\begin{aligned}\Delta\omega_{\rm CL} &= \sum_{\alpha=x,y,z}\frac{\partial\omega}{\partial E_\alpha}E_\alpha(t) + \sum_{\alpha,\beta=x,y,z}\frac{\partial^2\omega}{\partial E_\alpha\partial E_\beta}E_\alpha(t)E_\beta(t)\\ &= \sum_{\alpha,\beta=x,y,z}\frac{\partial^2\omega}{\partial E_\alpha\partial E_\beta}E_\alpha(t)E_\beta(t),\end{aligned} \tag{6}$$

where $E_\alpha(t)$ is the time-dependent electric field on the carbon atom obtained from the MD simulations. The first term in the expansion vanishes in Eq. (6) due to the symmetry of the CO_2 molecule. Coefficients $\partial^2\omega/\partial E_\alpha\partial E_\beta$ can be obtained by molecular orbital (MO) frequency computations by changing the applied electric field step by step. $\Delta\omega_{\rm LJ}$ is also expanded in terms of the LJ force up to the second order according to semiclassical perturbation theory:[22]

$$\begin{aligned}\Delta\omega_{\rm LJ} &= -\frac{f}{2\mu^2\omega_0^3}\frac{\partial V_{\rm LJ}(t)}{\partial Q} + \frac{1}{\mu\omega_0}\frac{\partial^2 V_{\rm LJ}(t)}{\partial Q^2}\\ &= \frac{1}{\mu\omega_0}\frac{\partial^2 V_{\rm LJ}(t)}{\partial Q^2},\end{aligned} \tag{7}$$

where f is the bond anharmonicity, μ is the reduced mass, ω_0 is the center frequency, $V_{\rm LJ}(t)$ is the time-dependent LJ potential, and Q is the normal coordinate. The first term again vanishes because there is no bond anharmonicity in the symmetric CO_2 molecule. The LJ force $\partial^2 V_{\rm LJ}(t)/\partial Q^2$ can be analytically calculated from the MD trajectory:

$$\frac{\partial^2 V_{\rm LJ}(t)}{\partial Q^2} = \sum_{i,j}\sum_{\alpha,\beta=x,y,z}\frac{\partial^2 V_{\rm LJ}(t)}{\partial r_{i\alpha}\partial r_{j\beta}}\frac{\partial r_{i\alpha}}{\partial Q}\frac{\partial r_{j\beta}}{\partial Q}. \tag{8}$$

The total instantaneous frequency [Eq. (5)] is substituted into Eq. (2) to give the final vibrational correlation function.

C. Raman band shape

A Raman band shape also includes both the vibrational and the rotational broadenings. The vibrational correlation function has the same form as that in the infrared band shape [Eq. (1)].[16] The rotational correlation function is different from that of the infrared. The Raman rotational correlation function of a linear molecule has the form:[18,19,23]

$$\phi_{\rm rot,Raman}(t) = \frac{1}{2}\langle 3\,[\mathbf{n}(t)\cdot\mathbf{n}(0)]^2 - 1\rangle. \tag{9}$$

The rotational and vibrational broadenings can be separated by polarized Raman measurements. In the framework of the polarizability approximation, the isotropic component $I_{\rm iso}$ and the anisotropic component $I_{\rm aniso}$ of a Raman band are given as follows:[24]

$$\begin{aligned}I_{\rm iso} &\propto I_{XX} - \tfrac{4}{3}I_{XZ}\\ I_{\rm aniso} &\propto I_{XZ},\end{aligned} \tag{10}$$

where I_{XX} and I_{XZ} are the observed polarized Raman scattering intensities, parallel and perpendicular, respectively, to the incident polarization. $I_{\rm iso}$ includes the pure vibrational broadening:

$$I_{\rm iso}(\omega) = \int_{-\infty}^{\infty} dt\,\exp(-i\omega t)\cdot\phi_{\rm vib}(t), \tag{11}$$

while $I_{\rm aniso}$ includes both the vibrational and rotational broadenings:

$$I_{\rm aniso}(\omega) = \int_{-\infty}^{\infty} dt\,\exp(-i\omega t)\cdot\phi_{\rm vib}(t)\cdot\phi_{\rm rot,Raman}(t). \tag{12}$$

D. Time-resolved infrared absorption anisotropy

A rotational correlation can also be measured directly in the time domain by anisotropic time-resolved spectroscopy. Time-dependent anisotropy $r(t)$ for a single initial state is defined as[25]

$$r(t) = \frac{N_{//}(t) - N_{\perp}(t)}{N_{//}(t) + 2N_{\perp}(t)}, \tag{13}$$

where $N_{//}(t)$ and $N_{\perp}(t)$ are the parallel and the perpendicular intensities of emission or absorption, respectively. The value $r(t)$ shows the time dependence expressed as

$$r(t) = \frac{1}{5}\langle 3[\boldsymbol{\mu}(0)\cdot\boldsymbol{\gamma}(t)]^2 - 1\rangle, \tag{14}$$

where $\boldsymbol{\mu}(0)$ is the transition dipole moment of the excitation and $\boldsymbol{\gamma}(t)$ is the transition dipole moment of the probing event (emission or absorption). In the case of the CO_2 antisymmetric stretch mode, both $\boldsymbol{\mu}(0)$ and $\boldsymbol{\gamma}(t)$ are parallel to the molecular axis $\mathbf{n}(t)$, and thus the time-dependence of $r(t)$ is similar to the Raman rotational correlation [Eq. (9)].

$$\begin{aligned} r(t) &= 0.4^* \frac{1}{2}\langle 3\,[\mathbf{n}(t)\cdot\mathbf{n}(0)]^2 - 1\rangle \\ &= 0.4^* \phi_{\text{rot, Raman}}\,(t). \end{aligned} \tag{15}$$

III. EXPERIMENTAL DETAILS

A. Infrared measurements

Infrared spectra have been recorded on a BOMEM DA-8 FT-Spectrometer with the following conditions: globar IR source, DTGS detector, KBr beam splitter, 4000–400 cm^{-1} spectral region, 1 cm^{-1} resolution, 16 times accumulation, Hamming apodization function, no zero-filling, 0.2 cm/s scan rate, and 10.0 mm aperture diameter. The sample chamber is evacuated to ~1 Torr in order to eliminate the effect of atmospheric CO_2 absorption. The sample solution is sealed into a laboratory-made cell consisting of two CaF_2 windows and a 25 μm lead spacer sealed together with epoxy resin. Commercially obtained acetonitrile (Wako, HPLC grade) is used without further purification. A dilute sample solution has been prepared by blowing CO_2 on the surface of acetonitrile (2 ml) for 10 s at a 1 l/min flow rate.

B. Computational methods

All MD simulations are performed using the GROMACS (Ref. 26) package. The system consists of eight CO_2 molecules and 1720 acetonitrile molecules. The rigid EPM2 model by Harris and Yung[27] is employed as the CO_2 model. The method originally proposed by Ciccotti[28] and applied to CO_2 by Huang *et al.*[29] is used to propagate the equations of motion of the rigid linear CO_2 molecule. The mass is redistributed into two dummy particles without any charge or LJ parameters. Charges and LJ parameters are kept on the carbon and oxygen sites, but no mass exists on these sites. The positions of the dummy particles are determined so as to give the same moment of inertia as that of the original EPM2 model. The all-atom and fully flexible model by Grabuleda *et al.*[30] is used for acetonitrile. Periodic boundary conditions are used with Particle Mesh Ewald (PME) to treat the long-range Coulomb interaction. For the van der Waals interaction, shift method is used with twin-range cutoff radius, and long range dispersion corrections are applied for energy and pressure. After 1 ns of equilibration by an NPT simulation with Berendsen coupling, an NVE production run of 1 ns is carried out.

MO computations have been done with the GAUSSIAN 09 (Ref. 31) package at MP2/6-31+G(d,p) level with FIELD option. Applied fields are set along the z axis (molecular axis) and the x axis (perpendicular to the z axis), each from 0 to 0.02 a.u. with a 0.002 a.u. step. The coefficients are found to be

$$\Delta\omega_{\text{CL}} = -2670E_x(t)^2 + 39E_x(t)E_z(t) + 4318E_z(t)^2, \tag{16}$$

where the frequency is in cm^{-1} and the electric field is in a.u.

C. Raman measurements

Polarized Raman scattering spectra have been measured with a laboratory-built Raman spectroscopic system.[32] The 532 nm output from a frequency-doubled Nd:YVO_4 laser operating in a single longitudinal mode illuminates the sample in a quartz rectangular cell. The laser power is 60 mW at the sample point. The polarization of the collected 90° scattered light is analyzed with a Glan-Thompson polarizer. The efficiency of the polarizer is estimated to be 99.9% by comparing the observed depolarization ratio of the totally symmetric ν_1 band of $C^{35}Cl_3{}^{37}Cl$ (0.0047) to the reported value (0.0032).[33] After eliminating Rayleigh scattered light by an edge filter (Semrock), the scattered light is introduced into a multi-channel spectrometer consisting of a single polychromator ($f = 60$ cm, F/6.2, NR-1800, JASCO) with a 1200 grooves/mm grating and a liquid nitrogen cooled CCD camera (Spec-10, Princeton instruments). The slit width is set to 60 μm, which gives a pseudo-Gaussian instrument function with a bandwidth of 1.1 cm^{-1} (HWHM). Commercially obtained acetonitrile (Nacalai Tesque, fluorescence grade) is used without further purification. The solvent is saturated with CO_2 by bubbling over 2 min at a 1 l/min flow rate.

D. Time-resolved infrared measurements

Sub-picosecond time-resolved infrared spectroscopy measurements have been carried out with a laboratory-built system. Infrared pulses are generated by difference frequency generation (DFG) from the near-IR signal and idler outputs of an optical parametric amplifier (OPerA, Coherent) pumped by an amplified Ti:Sapphire laser (Integra-C, Quantronix). The infrared light is divided into three as the pump, probe, and reference beams, respectively. The pump light is modulated by a chopper, goes through an optical delay and a half wave plate, and then focused on the sample by a lens. Probe and reference beams are introduced to the sample by a parabolic mirror. The probe and reference beams are

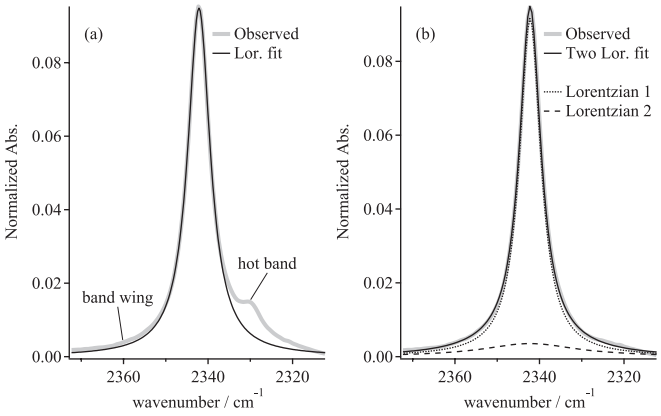

FIG. 1. The observed infrared band shape of CO_2 antisymmetric stretch mode in acetonitrile: (a) the observed band (thick gray line) and its single Lorentzian fit (thin black line) and (b) the observed band (thick gray line, hot band subtracted) and its curve fit (thin solid line) by the sum of two Lorentzians (dashed and dotted lines).

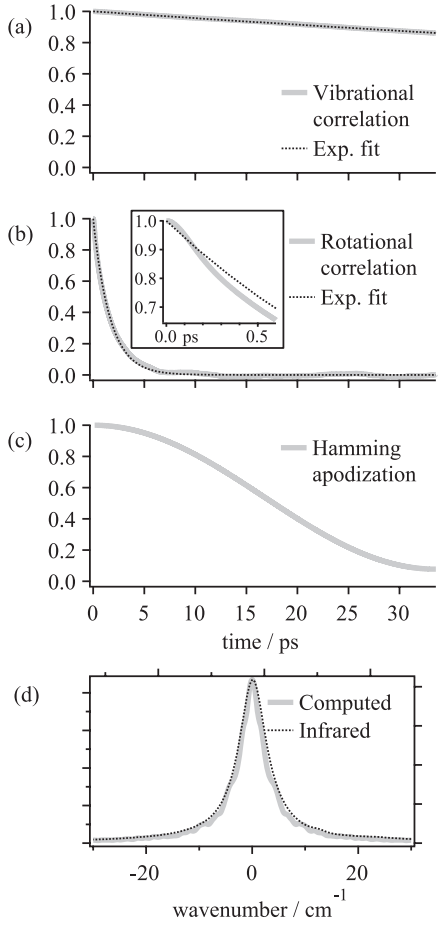

FIG. 2. Computed correlation functions and the corresponding band shape by the MD simulation: (a) the vibrational correlation function (solid) and its single exponential fit (dotted), (b) the rotational correlation function (solid) and its single exponential fit (dotted), (c) a Hamming apodization function and (d) the computed band shape (solid) and the observed (dotted) infrared band shape.

then guided to a two-channel monochromator equipped with two MCT detectors. The signals are integrated by a boxcar integrator and then collected. Isotope substituted $^{13}CO_2$ (SI Science, 99%) is used in order to avoid the interference from atmospheric CO_2. Ethanol (Wako, 99.5%) is used as an alternative solvent which has less band overlap with CO_2. The steady-state infrared absorption bandwidth of $^{12}CO_2$ in ethanol shows a bandwidth similar to that in acetonitrile. The sample solution is flowed through a laboratory-made cell (100 μm spacer) by a roller pump and kept bubbled by $^{13}CO_2$ (~50 ml/min) throughout the measurement.

IV. RESULTS AND DISCUSSION

A. Infrared band shape analysis

Figure 1(a) shows the observed infrared band shape of CO_2 antisymmetric stretch band in acetonitrile (gray line) together with a least-squares fit Lorentzian curve (black thin line). The overall band shape is non-Lorentzian, with broad band wings that cannot be reproduced with a single Lorentzian function. This fact indicates that a non-exponential decay dominates the vibrational and/or rotational correlation functions. The small side band located around 2325 cm^{-1} is assigned to a hot band due to the bending mode through temperature dependence measurements. This feature is subtracted prior to the following analysis. The band shape is well fitted with a sum of two Lorentzians located at the same center position [Fig. 1(b)]. The bandwidths (HWHM) of the two Lorentzians are 3.193 ± 0.003 and 21.1 ± 0.8 cm^{-1}, respectively, and the intensity ratio of the two bands is 4.39:1. (The error indicates one standard deviation obtained in least-squares fitting analysis; the same shall apply hereafter.)

B. Computation of the band shape

Figure 2 shows the vibrational ((a), gray solid line) and rotational ((b), gray solid line) correlation functions obtained by the computational method described in Sec. III B, along with a Hamming apodization function (c) that gives the same instrument function as in the FT-IR measurements. Figure 2(d) shows the band shape calculated by multiplying the two correlation functions and the apodization function, followed by a Fourier transformation (gray solid line). The observed infrared band shape (black dotted line) is very well reproduced, including the broad band-wing feature. Surprisingly, vibrational correlation is retained over a few tens of picoseconds. A single exponential curve fit ((a), dotted line) gives a decay constant of 224.99 ± 0.01 ps, which corresponds to a Lorentzian of 0.02356 cm^{-1} bandwidth (HWHM). This decay constant is significantly larger than the reported population decay lifetime (10 ps in water[34]). However, 10 ps lifetime corresponds to a Lorentzian of 0.5 cm^{-1} bandwidth, which is still small compared to the observed bandwidth of 3.193 and 21.1 cm^{-1}. There is also a possibility that CO_2 has longer vibrational energy lifetime in acetonitrile than in water, since antisymmetric stretch mode of the neutral linear triatomic molecule N_2O has longer lifetime in hydrocarbons (55 ps) than in water (9 ps).[35] In contrast, rotational correlation decays in a few picoseconds. A single exponential curve fit ((b), dotted line) gives a decay constant of 1.6462 ± 0.0008 ps, which corresponds to a Lorentzian of

3.2249 cm^{-1} bandwidth. This suggests that the total band broadening is almost purely rotational, while the broadening due to vibrational dephasing is less than 1% of the total bandwidth.

There is a rapid decrease in the rotational correlation for the first few tenths of picosecond [inset of Fig. 2(c)], corresponding to the broad band wings in the frequency domain. This decay feature in the rotational correlation cannot be treated with diffusion equations, which give a single exponential decay. The diffusion equation applied to the rotational motion assumes "small angular steps." For small molecules such as CO_2, these small steps may not be applicable. Gordon[36] has shown more generalized rotational diffusion models called the m-diffusion model and the *J*-diffusion model. They can treat both small angular steps and large angular steps over $\pi/2$. Basically, the models are the rotors having stochastically changing angular frequencies with no reorientation.

FORTRAN 90 programs have been written to simulate the rotational correlation functions of the m-diffusion model, instead of solving recursive equations as done by Gordon. A rotor rotates freely with a constant angular frequency ω [rad s^{-1}]. The direction of the angular momentum is stochastically changed with a probability of τ^{-1} [s^{-1}]. The amplitude of ω and the orientation of the rotor are unchanged during the change. Correlation functions are calculated for 50 different ω's for one τ, and they are summed up according to the Maxwell-Boltzmann distribution.

Figure 3(a) shows the resultant correlation function with $\tau = \infty$, 0.7, 0.2, 0.08, and 0.04 ps from the bottom, respectively. Free rotor ($\tau = \infty$) shows a negative correlation, which means the molecule rotates over $\pi/2$. With increasing probability of diffusion, the negative peak disappears, whereas the rapid decrease in the first few tenths of picosecond remains as a damped oscillation. This feature resembles the correlation function obtained in the MD simulation [Fig. 3(b)]. The observed broad band wings are therefore attributed to the damped oscillatory rotation; the CO_2 molecule being small, it rotates in large angle steps during diffusion.

C. Raman band shape analysis

Figure 4(a) shows the observed parallel (I_{XX}, solid line) and perpendicular (I_{XZ}, dotted line) Raman spectra of the CO_2 symmetric stretch mode in acetonitrile. This mode is in a Fermi resonance with the second overtone of the bending mode with a splitting over 100 cm^{-1}. Only the band at 1275 cm^{-1} is analyzed, since the other band observed at 1382 cm^{-1} overlaps with a strong solvent band. The effect of Fermi resonance in the band shape is not taken into account in the analysis. The small band at 1255 cm^{-1} is due to $^{13}CO_2$ and is subtracted prior to the following analysis. The isotropic (I_{iso}) and anisotropic (I_{aniso}) Raman spectra are calculated as follows. The isotropic spectrum is obtained by subtracting the perpendicular spectrum times 0.75 from the parallel. The anisotropic spectrum is considered to be the same as the perpendicular spectrum.

Figure 4(b) shows the calculated I_{iso} (gray circle) and I_{aniso} (black circle) spectra and their least-squares fit by Voigt functions (gray and black lines, respectively). The Gaussian component of the Voigt function is set to be the slit function, assuming that the vibrational and rotational broadenings are Lorentzians. The best fit Lorentzian bandwidths (HWHM) are 1.29 ± 0.01 for I_{iso} and 7.2 ± 0.3 cm^{-1} for I_{aniso}, respectively.

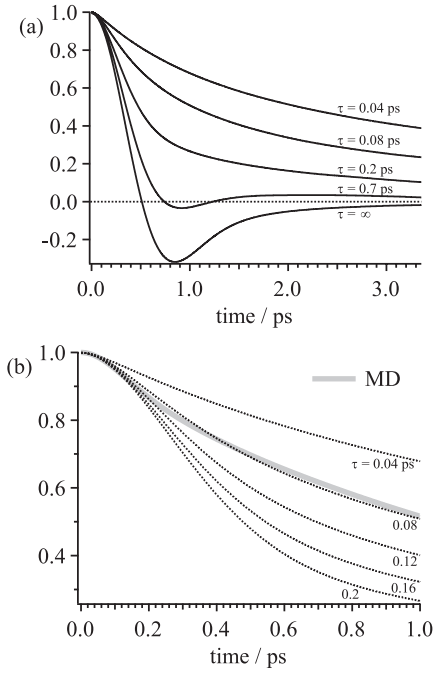

FIG. 3. Rotational correlation functions obtained by the m-diffusion model: (a) $\tau = \infty$, 0.7, 0.2, 0.08, 0.04 ps from the bottom to top and (b) rotational correlation function of CO_2 in acetonitrile by the MD simulation (gray solid line) and correlation functions by the m-diffusion model (black dotted line) with $\tau = 0.2$, 0.16, 0.12, 0.08, 0.04 ps from the bottom to top.

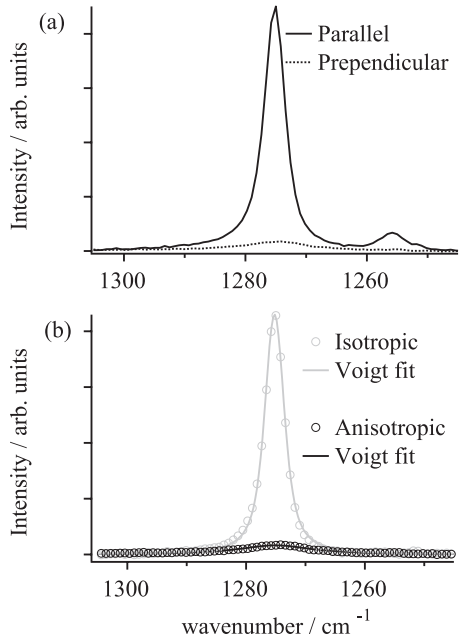

FIG. 4. The observed Raman band shape of CO_2 symmetric stretch mode in acetonitrile: (a) the observed parallel (I_{XX}, solid) and perpendicular (I_{XZ}, dotted) scattering intensities and (b) the calculated isotropic (I_{iso}, gray circle) and anisotropic (I_{aniso}, black circle) components, and their Voigt function fits (gray and black solid lines, respectively).

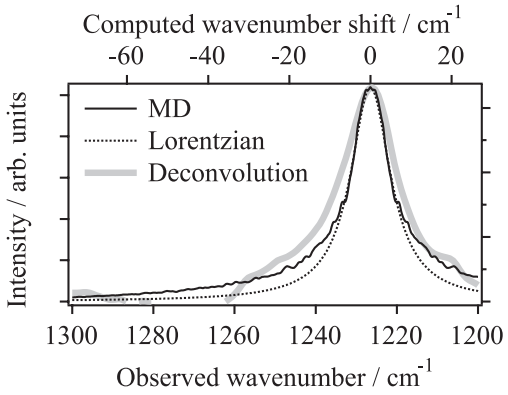

FIG. 5. Raman rotational broadening calculated by the Lorentzian approximation (dotted line) and by the direct deconvolution of I_{aniso} by I_{iso} (thick gray line), compared to the MD simulation (black line).

The rotational broadening can be calculated by deconvolving I_{aniso} by I_{iso} according to Eqs. (11) and (12). If both the vibrational and the rotational broadenings are assumed to be Lorentzians, the rotational broadening has a bandwidth of $7.2 - 1.2 = 6.0\ cm^{-1}$. Figure 5 shows a Lorentzian with HWHM of 6 cm^{-1} (dotted line) and a rotational correlation function computed from the MD simulation according to Eq. (9) (black solid line). They seem to agree with each other, except that the band-wing feature cannot be reproduced as long as Lorentzian band shapes are assumed in the Raman analysis. Direct deconvolution of I_{aniso} by I_{iso} is also attempted (thick gray solid line in Fig. 5) using the Wiener filtering algorithm.[37] The resultant spectrum also seems to be in good agreement with the MD simulation result, although it is too noisy to determine the bandwidth. Nevertheless, the rotational correlation function computed from the MD simulation has a correlation time consistent with the polarized Raman experiment, supporting the result that the observed infrared band shape is determined almost solely by rotational dephasing.

D. Time-resolved infrared absorption anisotropy analysis

Figure 6(a) shows the observed time-resolved parallel (filled circle) and perpendicular (open circle) infrared absorptions of $^{13}CO_2$ in ethanol. The steady-state infrared absorption bandwidths of $^{12}CO_2$ in ethanol obtained by the two-Lorentzian fitting are similar to those in acetonitrile; bandwidth of 3.246 ± 0.007 (3.193 ± 0.003 in acetonitrile) and 14.2 ± 0.1 (21.1 ± 0.8) cm^{-1} with the intensity ratio of 3.57:1 (4.39:1). The isotope substitution does not alter the moment of inertia, since the carbon atom is located on the axis of the rotation. The anisotropy r is calculated using Eq. (13), and its time dependence is shown in Fig. 6(b) (circle). Curve fitting by a single exponential function [Fig. 6(b), solid line] gives a decay constant of 0.9 ± 0.1 ps, which corresponds to a Lorentzian of 5.5 ± 0.8 cm^{-1} bandwidth (HWHM) in the frequency domain. This value is in good agreement with the observed rotational Raman broadening (6.0 cm^{-1}) and the rotational broadening estimated by the MD simulation. It is thus supported further that the observed infrared band shape

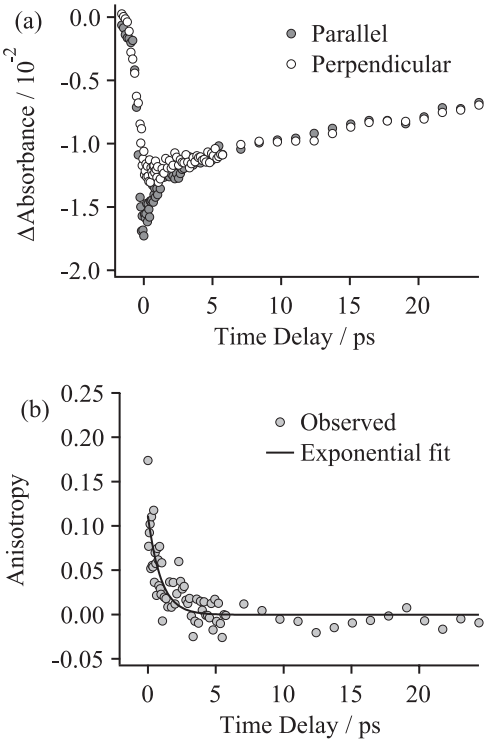

FIG. 6. The observed time-resolved infrared absorption anisotropy: (a) parallel (filled circle) and perpendicular (open circle) absorptions of $^{13}CO_2$ in ethanol and (b) the calculated anisotropy (circle) and its single exponential fit (line).

of CO_2 is determined predominantly by pure rotational dephasing.

V. CONCLUSION

A comprehensive study on the rotational behavior of solvated CO_2 has been carried out including an infrared band shape analysis, a theoretical simulation, a polarized Raman band shape analysis, and a time-resolved infrared absorption anisotropy analysis. The observed infrared band is non-Lorentzian shaped with broad band wings. The band shape computed with a combined method of MD simulations and quantum chemical calculations reproduces the observed infrared band shape. According to the simulation, the infrared band shape is determined by almost pure rotational dephasing, while the contribution from the vibrational broadening is less than 1% of the total bandwidth. The rapid decrease in the rotational correlation in the first few tenths of picosecond, which gives rise to the observed broad band wings, has been shown to correspond to the damped oscillatory behavior of the rotational dynamics of CO_2. The CO_2 molecule being relatively small, it rotates in large angle steps during rotational diffusion. This characteristic rotational behavior has been observed clearly in the vibrational band shape of CO_2 because the molecule is non-polar and therefore the vibrational dephasing is too slow to give large bandwidths that can mask the weak broad feature due to the fast rotational decay. Polarized Raman scattering and time-resolved infrared absorption anisotropy have been measured in order to confirm the observed broad rotational bandwidth. The obtained Raman

rotational broadening and the infrared anisotropy correlation are consistent with the computed correlation function. It is strongly supported that the band shape of CO_2 antisymmetric stretch mode is mostly dominated by the characteristic rotational dynamics elucidated in the theoretical simulation, since all the results including three spectroscopies and theoretical simulations agree with one another.

ACKNOWLEDGMENTS

All MD simulations have been performed at Department of Chemistry, The University of Iowa. The authors thank Professor Claudio J. Margulis for much useful advice on simulations. All MO computations have been performed using Research Centre for Computational Science, Okazaki, Japan.

[1]W. G. Rothschild, J. Chem. Phys. **65**, 455 (1976).
[2]D. W. Oxtoby, Ann. Rev. Phys. Chem. **32**, 77 (1981).
[3]S. Bratos, G. Tarjus, and P. Viot, J. Chem. Phys. **85**, 803 (1986).
[4]R. A. MacPhail, R. G. Snyder, and H. L. Strauss, J. Chem. Phys. **77**, 1118 (1982).
[5]P. J. W. Debye, *Polar molecules* (Dover, New York, 1929).
[6]F. Perrin, J. Phys. Radium **5**, 497 (1934).
[7]H. Greaner, G. Seifert, and A. Laubereau, Chem. Phys. Lett. **172**, 435 (1990).
[8]M. Li, J. Owrutsky, J. P. Culver, A. Yodh, and R. M. Hochstrasser, J. Chem. Phys. **98**, 5499 (1993).
[9]F. C. Frank, Trans. Faraday Soc. **32**, 1634 (1936).
[10]W. Kauzmann, Rev. Mod. Phys. **14**, 12 (1942).
[11]J. G. Powles and D. K. Green, Phys. Lett. **3**, 134 (1962).
[12]S. P. Wang and M. Schwartz, J. Mol. Liquids **47**, 121 (1990).
[13]G. Van der Zwan and J. T. Hynes, J. Phys. Chem. **89**, 4181 (1985).
[14]M.-L Horng, J. A. Gardecki, and M. Maroncelli, J. Phys. Chem. A **101**, 1030 (1997).
[15]P. Padilla and S. Toxvaerd, J. Chem. Phys. **94**, 5650 (1991).
[16]D. W. Oxtoby, Adv. Chem. Phys. **40**, 1 (1979).
[17]*Basic Modern Physics 5, Statistical Physics (Toukei Butsurigaku)* edited by M. Toda and R. Kubo (Iwanami Shoten, Japan, 1978).
[18]R. G. Gordon, J. Chem. Phys. **43**, 1307 (1965).
[19]W. A. Steele, Adv. Chem. Phys. **34**, 1 (1976).
[20]R. Kubo, Adv. Chem. Phys. **15**, 101 (1969).
[21]T. Hayashi and H. Hamaguchi, Chem. Phys. Lett. **326**, 115 (2000).
[22]D. W. Oxtoby, D. Levesque, and J.-J. Weis, J. Chem. Phys. **68**, 5528 (1978).
[23]R. G. Gordon, J. Chem. Phys. **42**, 3658 (1965).
[24]*Raman Spectroscopy*, edited by H. Hamaguchi and A. Hirakawa (Gakkai Shuppan Center, Japan, 1988).
[25]G. R. Fleming, *Chemical Applications of Ultrafast Spectroscopy* (Oxford University Press, New York, 1986).
[26]H. J. C. Berendsen, D. van der Spoel, and R. van Drunen, Comput. Phys. Commun. **91**, 43 (1995).
[27]J. G. Harris and K. H. Yung, J. Phys. Chem. **99**, 12021 (1995).
[28]G. Ciccoti, Mol. Phys. **47**, 1253 (1982).
[29]X. Huang, C. J. Margulis, Y. Li, and J. Berne, J. Am. Chem. Soc. **127**, 17842 (2005).
[30]X. Grabuleda, C. Jaime, and P. A. Kollman, J. Comput. Chem. **21**, 901 (2000).
[31]M. J. Frisch, G. W. Trucks, H. B. Schlegel *et al.* GAUSSIAN 09, Revision A.1, Gaussian, Inc., Wallingford, CT, 2009.
[32]H. Okajima and H. Hamaguchi, Appl. Spectrosc. **63**, 968 (2009).
[33]W. Kiefer and J. A. Topp, Appl. Spectrosc. **28**, 26 (1974).
[34]P. Hamm, M. Lim, and R. M. Hochstrasser, *Ultrafast Phenomena XI*, edited by T. Elsaesser, J. G. Fujimoto, D. Wiersma, and W. Zinth (Springer, Berlin, 1988), p. 514.
[35]L. R. Chieffo, J. T. Shattuck, E. Pinnick, J. J. Amsden, M. K. Hong, F. Wang, S. Erramilli, and L. D. Ziegler, J. Phys. Chem. B, **112**, 12776 (2008).
[36]R. G. Gordon, J. Chem. Phys. **44**, 1830 (1966).
[37]N. Wiener, *Extrapolation, Interpolation and Smoothing of Stationary Time Series* (Wiley, New York, 1949).